Journal of Catalysis 285 (2012) 160–167

Contents lists available at SciVerse ScienceDirect

Journal of Catalysis

journal homepage: www.elsevier.com/locate/jcat

Investigation of the structure and activity of $VO_x/CeO_2/SiO_2$ catalysts for methanol oxidation to formaldehyde

William C. Vining, Jennifer Strunk, Alexis T. Bell *

Chemical Sciences Division, Lawrence Berkeley National Laboratory and Department of Chemical and Biomolecular Engineering, University of California, Berkeley, CA 94720-1462, United States

ARTICLE INFO

Article history:
Received 1 July 2011
Revised 20 September 2011
Accepted 22 September 2011
Available online 22 October 2011

Keywords:
Methanol oxidation
Vanadia
Ceria
Silica

ABSTRACT

The effect of ceria on the partial oxidation of methanol to formaldehyde over $VO_x/CeO_2/SiO_2$ catalysts was investigated. A two-dimensional layer of ceria on silica was prepared by grafting cerium (IV) *t*-butoxide ($Ce(OC_4H_9)_4$) onto high surface area, mesoporous silica, SBA-15, and then calcining the resulting product in air at 773 K. Ce surface concentrations obtained this way ranged from 0.2 to 0.9 Ce nm^{-2}. Next, V was introduced by grafting $VO(O^iPr)_3$ onto CeO_2/SiO_2 in order to achieve a surface concentration of 0.6 V nm^{-2}. XANES spectra indicate that all of the V is in the 5+ oxidation state and Raman spectra show that vanadia exist as pseudo-tetrahedra bonded to either silica or ceria. Data from Raman spectroscopy and temperature-programmed desorption of adsorbed methanol indicate that with increasing Ce surface density, most of the V becomes associated with the deposited ceria. The turnover frequency for methanol oxidation is nearly two orders of magnitude higher for $VO_x/CeO_2/SiO_2$ than for VO_x/SiO_2, whereas the apparent activation energy and apparent first-order pre-exponential factor are 17 kcal/mol and 1.4×10^6 mol CH_2O (mol V atm s)$^{-1}$, respectively, for $VO_x/CeO_2/SiO_2$ and 23 kcal/mol and 2.3×10^7 mol CH_2O (mol V atm s)$^{-1}$, respectively, for VO_x/SiO_2.

1. Introduction

The catalytic activity of supported vanadia shows significant differences as a function of support composition [1–6]. These differences are well documented for the case of oxidation of methanol to formaldehyde, where the rate of CH_2O formation has been shown to proceed more rapidly by over an order of magnitude when vanadia is supported on titania, zirconia, or ceria than on silica [1,6–8]. A similar increase in activity for the oxidation of methanol to formaldehyde is seen for bilayered catalysts in which TiO_x or ZrO_x is grafted in submonolayer quantities onto silica [4,5,9,10]. Despite many attempts to understand the origin of this support effect, a consensus regarding the cause(s) has not emerged [1–5,9–15]. In order to elucidate the mechanism by which the support composition affects the activity of the supported vanadate species, the underlying support surface must be thoroughly characterized. Careful characterization of the supported vanadia layer is also important to understand how the different vanadia structures impact the reaction rate.

A number of investigators have found it advantageous to use silica as the support material and to graft the modifying oxide (e.g., TiO_x, ZrO_x) layer onto the silica. If the modifying layer is deposited using an organometallic precursor, it can react with surface silanol groups to form an amorphous, two-dimensional oxide layer. Either isolated monovanadate or polyvanadate species can then be grafted onto such a modified support, with most of the vanadate species becoming attached to the modifying layer [9,10,4,5]. Until recently, attempts to carry out similar studies with $VO_x/CeO_2/SiO_2$ have been hampered by the difficulty of dispersing ceria as a two-dimensional layer; therefore, most of what is known about the effects of ceria on the activity of vanadia for the oxidation of methanol has come from studies of $VO_x/CeO_2/SiO_2$ in which the ceria is present as nanoparticles of CeO_2 and from studies of vanadia supported on bulk ceria.

Previous studies of bilayered $VO_x/CeO_2/SiO_2$ catalysts have focused on the characterization of oxide phases by Raman spectroscopy but have not identified how ceria promotes the activity of vanadia [16–19]. Studies by Vohs and coworkers of methanol oxidation on vanadia supported on polycrystalline CeO_2 [20,21] and on the (1 1 1) surface of monocrystalline CeO_2 [22,21,23] have shown that the rate-limiting step in the formation of formaldehyde involves the transfer of a H atom from the methyl group of adsorbed methoxy species bonded to ceria-supported vanadate species. Abbott et al. have also investigated methanol oxidation over vanadia supported on CeO_2(1 1 1) thin films [24]. The authors propose that Ce^{3+} adjacent to isolated vanadate structures are responsible for the increased reactivity for methanol oxidation but do not fully explain how these centers contribute to the reaction. Insight into the structure of ceria-supported vanadia has been provided by DFT carried

* Corresponding author.
E-mail addresses: bell@cchem.berkeley.edu, alexbell@berkeley.edu (A.T. Bell).

0021-9517/$ - see front matter © 2011 Elsevier Inc. All rights reserved.
doi:10.1016/j.jcat.2011.09.024

out by Metiu and coworkers and Sauer and coworkers [25,26]. Both sets of authors find that isolated vanadate species on CeO_2 (1 1 1) can exist in at least two types of distorted tetrahedral environments.

In the present study, we extend our earlier work on methanol oxidation catalyzed by vanadate species supported on silica and on two-dimensional layers of titania and zirconia supported on silica [3–5]. This effort was enabled by our recent studies showing amorphous, two-dimensional layers of ceria can be deposited onto silica using cerium (IV) *t*-butoxide as the precursor [27]. In all cases, the surface density of vanadia was maintained low enough so that large aggregates of vanadia were not observed. The catalysts were characterized by Raman and UV–Visible spectroscopy, and X-ray absorption near-edge spectroscopy (XANES). The catalytic properties of $VO_x/CeO_2/SiO_2$ catalysts were studied using methanol as a probe molecule. Our results indicate that the ceria domain participates in the reaction by providing an alternative mechanism for H-abstraction from adsorbed methoxy species in the rate-determining step leading to formaldehyde. The results obtained with $VO_x/CeO_2/SiO_2$ are compared with those reported in our earlier work on $VO_x/TiO_2/SiO_2$ and $VO_x/ZrO_2/SiO_2$. It is noted that the catalytic activity and the apparent rate parameters for $VO_x/TiO_2/SiO_2$, $VO_x/ZrO_2/SiO_2$, and $VO_x/CeO_2/SiO_2$ are very similar, but differ significantly from those for VO_x/SiO_2.

2. Experimental methods

SBA-15, a high surface area mesoporous silica, was synthesized according to the method described in Refs. [27,28]. Briefly, Pluronic P123 (<MW> = 5800) was suspended in water and stirred for 1.5 h, then 120 cm^3 of 2 M HCl was added and the resulting mixture stirred for an additional 2 h. Next, tetraethyl orthosilicate (TEOS) was added dropwise while the mixture was held at 308 K and stirred for 24 h. Stirring was stopped, and the mixture was heated at 373 K for 24 h. The precipitate was filtered and washed six times with deionized water and once with 50 cm^3 of acetone. After drying overnight in air, the filtrate was heated to 773 K in air at 2 K min^{-1} and held for 4 h.

Cerium was grafted onto SBA-15 using cerium (IV) *t*-butoxide ($Ce(OC_4H_9)_4$, Gelest), as described in Ref. [27]. The $Ce(O^tBu)_4$ was dissolved in 70 cm^3 of anhydrous toluene at ambient temperature in an inert atmosphere before mixing with the SBA-15 support. The liquid was removed and the resulting sample rinsed three times with anhydrous toluene before drying at ambient temperature under vacuum. The samples were then heated to 573 K in He, after which the gas was switched to synthetic air, and the sample heated to 773 K for 4 h.

Vanadium was grafted onto CeO_x/SiO_2, in a single grafting step, using $VO(O^iPr)_3$ (Alpha, 96% pure) as the vanadium precursor. The desired quantity of vanadium is mixed with ~60 cm^3 of anhydrous toluene in a dry N_2 atmosphere before mixing with the support after drying under vacuum at 393 K for 4 h [4,5]. After stirring at ambient temperature for 4 h, the sample was rinsed three times with anhydrous toluene before treating in synthetic air at 823 K for 6 h. The resulting catalysts were stored in a glove box without exposure to the atmosphere.

$CeVO_4$ was synthesized by mixing $Ce(NO_3)_3{\cdot}6H_2O$ and vanadyl acetylacetonate together with a mortar and pestle in a 1:1 molar ratio before treating in synthetic air to 1023 K for 8 h. The resulting product was dark purple.

The surface area of SBA-15 before and after cerium grafting were determined by nitrogen physisorption at 77 K using an Autosorb-1 instrument (Quantachrome) using the single-point BET method. The weight percentage of cerium and vanadium was determined using inductively coupled plasma (ICP) analysis by Galbraith Laboratories. The apparent surface densities of Ce and V were calculated based on the surface area after Ce grafting.

Raman spectra were acquired using a Jobin Yvon-Horiba spectrometer equipped with a confocal microscope and a 532-nm Nd:YAG laser. Prior to the acquisition of Raman spectra, samples were sealed in a sample holder in the glove box. Eight scans of 4 s each were acquired at room temperature using 15 mW of laser power at the sample.

V K-edge and Ce L_{III}-edge XAS measurements were performed at the Advanced Photon Source (APS) on beamline 10-BM using a Si(1 1 1) monochromator crystal. The beam was detuned by 50% at the V K-edge. All scans were taken in transmission mode using 20-cm ionization chambers filled with 85% N_2/15% He in I_0 (before the sample) and 60% N_2/40% Ar in I_t (after the sample). A reference V foil was placed after the sample for energy calibration. Scans were collected with a hold time of 1 s and a step size of 0.5 eV from 5455 to 5505 eV, 10 eV to 5705 eV , and 0.5 eV to 5750 eV. The sample mass was adjusted to obtain an absorbance of 2.5 and boron nitride was added, as needed, to form a self-supporting pellet. The sample cell is a continuous-flow glass tube reactor (length, 18 in.; diameter, 0.75 in.) isolated from the atmosphere with polyimide windows and stainless steel valves fitted at both ends.

The XAS data were analyzed with the IFEFFIT software and its complementary GUI Athena [29,30]. The edge energy was defined as the first inflection point after any pre-edge feature. The V K-edge XANES data were normalized by subtracting a pre-edge line fit to the data from −26.5 to −18 eV relative to the edge energy and a quadratic polynomial (k weight = 2) fit to the data from 41 to 224.5 eV relative to the edge energy.

An *in situ* XANES experiment was performed in order to identify the effects of temperature and gas composition on the oxidation states of V and Ce. This experiment was initiated by heating the catalyst pellet to 600 K in 60 cm^3 min^{-1} He. While held at 600 K, the gas flow was switched to 60 cm^3 min^{-1} 5000 ppm MeOH/He until no changes were observed in the V K-edge or Ce L_{III}-edge XANES. The catalysts were then heated at 773 K in the same MeOH/He flow and scans acquired until no changes were observed in the resulting spectra. Finally, 60 cm^3 min^{-1} of 10% H_2/He was passed over the catalyst until the XANES spectra exhibited no changes at 773 K. The extent of reduction of V was determined by carrying out V K-edge linear combination analysis (LCA) using the scan at 300 K in He and the scan after 773 K in 5000 ppm methanol as reference spectra to represent the fully oxidized (V^{5+}) and reduced catalyst, respectively. The data were fit from −20 to 30 eV relative to the edge energy using Athena. For ceria, the extent of reduction from Ce^{4+} to Ce^{3+} was performed using the peak intensity at 5727 eV for the Ce L_{III}-edge. This peak height was normalized by the values obtained from the reference spectra at 300 K in He and after treatment in 5000 ppm methanol at 773 K to represent Ce^{4+} and Ce^{3+}, respectively.

Diffuse reflectance UV–Visible spectra were recorded using a Harrick Scientific diffuse reflectance attachment (DRP) with a reaction chamber (HVC-DRP) and a Thermo Scientific Evolution 300 spectrophotometer. The spectra were acquired after loading the samples in the glove box at ambient temperature without exposing the sample to the atmosphere. The edge energy was calculated using Tauc's law for indirect transitions in amorphous and crystalline semiconductors [31]. In this expression, a straight line is fit through a plot of $[A \cdot h\nu]^{1/2}$ versus $h\nu$, where A is the absorbance and $h\nu$ is the incident photon energy. The x-intercept of this linear fit is the reported edge energy.

Temperature-programmed reaction (TPR_x) experiments were performed using a mixture of approximately 25 mg of catalyst and 25 mg of bare SBA-15. The mixture was placed in a quartz reactor and supported with quartz wool. The sample was

heated at 4 K min^{-1} to 773 K in a flow of high purity O_2 in He (20% O_2/He) flowing at 60 cm^3 min^{-1} and then held at 773 K for 1 h. Next, the sample was cooled in this gas mixture to 363 K, after which a mixture of 4% MeOH/7.5% O_2/He was flowed over the catalyst for 10 min at 363 K before the reactor temperature was increased at 2 K min^{-1} to 823 K. The reactor effluent was analyzed with a MKS Cirrus mass spectrometer. The concentrations of species formed were analyzed using a matrix-deconvolution method with calibrated response factors.

Temperature-programmed desorption (TPD) profiles were acquired using a pretreatment procedure similar to that used for TPR_x, except upon cooling to 363 K, the reactor was purged with He until no O_2 was observed. Next, 30 cm^3 min^{-1} of 4% MeOH/He was passed over the catalyst for 3 min, and the reactor purged in 30 cm^3 min^{-1} He for 45 min. After the purge, the reactor was heated at 4 K min^{-1} to 773 K and the effluent analyzed by a MKS Cirrus mass spectrometer as for the TPR_x data.

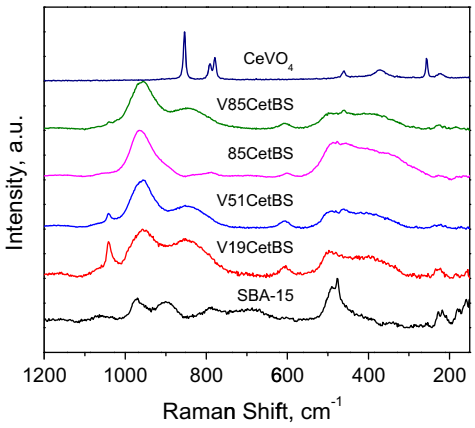

Fig. 1. Raman spectra of VCetBS catalysts after treating in syn. air to 773 K for 4 h. Spectra of the bare SBA-15 support, CeVO4, and 85CetBS are also included.

3. Results and discussion

3.1. Catalyst characterization

The names and BET surface areas of all samples are reported in Table 1. The number after V and before Ce gives the Ce surface coverage, the letters, tB, after Ce correspond to the $Ce(O^tBu)_4$ precursor, and the final letter, S, refers to the support, SBA-15. After ceria grafting, the surface area per gram of silica decreased for all samples the diameter of the mesopores and partially blocked the micropores of SBA-15 [27]. The vanadium surface density was held constant at ~0.6 V nm^{-2}, while the ceria layer density was increased from 0.2 to 0.9 Ce nm^{-2}. Assuming a monolayer coverage of 7 M nm^{-2} (M = V, Ce), both the V and Ce surface coverages are ⩽0.1 of a monolayer.

3.1.1. Raman

The Raman spectra for the catalysts are shown in Fig. 1. The spectrum for SBA-15 shows a strong band near 470–500 cm^{-1}, weak bands at 670 cm^{-1} and 800 cm^{-1}, and more intense bands at 900 and 970 cm^{-1}. The two peaks at 470 and 670 are due to the breathing modes of the silica [32], while the higher frequency peaks are due to Si—OH vibrational modes [33].

Sample 85CetBS in Fig. 1 is illustrative of the Raman spectrum taken after Ce grafting. No evidence of crystalline CeO_2 is observed, except for a weak band at 455 cm^{-1} for the highest surface density [27]. However, a new band is observed centered at 950 cm^{-1}, which grows with Ce surface coverage. This peak is, therefore, attributed to Ce—O—Si vibrations. The position of this feature is similar to that observed at 963 cm^{-1} in the infrared spectra of cerium oxides incorporated into mesoporous silica [34]. A broad peak is also observed in the region of 300–450 cm^{-1}, which could be a result of breathing modes of ceria present on the surface silica, since this region corresponds to similar vibrations in SiO_2 [32].

Upon grafting of V, peaks appear at 1040 and 850 cm^{-1}. The feature at 1040 cm^{-1} is due to the V=O stretch for pseudo-tetrahedral vanadate species, but definitive assignment of this feature is difficult for the following reasons. Isolated vanadate species grafted on silica have been observed to exhibit a V=O vibration in the region of 1035 to 1043 cm^{-1} [3,19,35,36]. However, a similar band for V=O vibrations has been observed in the region from 1022 to 1039 cm^{-1} for isolated vanadate species supported on bulk ceria [1,37]. Likewise, theoretical calculations of the vibrational spectrum for isolated pseudo-tetrahedral vanadates present on CeO_2(1 1 1), Structure A in Fig. 2, show that the V=O band for such species should be in the range of 1040 to 1046 cm^{-1} [25,38]. For these reasons, the position of the band at 1040 cm^{-1} cannot be used to differentiate between pseudo-tetrahedral vanadia bound to silica or ceria. Interestingly, the intensity of this peak decreases in intensity with increasing Ce surface density. Therefore, we believe that the peak at 1040 cm^{-1} is most likely due to the presence of pseudo-tetrahedral vanadate species bonded to silica. This assignment is supported by information derived from methanol temperature-programmed desorption (TPD) data (see below).

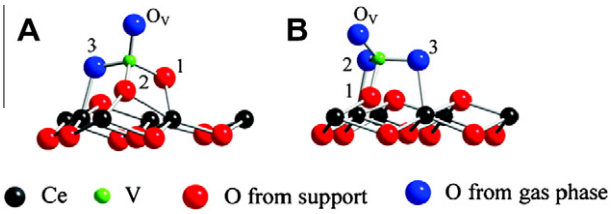

Fig. 2. VO_x structures on CeO_2 (1 1 1) surface as determined by density functional theory calculations: VO_2 (A) and VO_3 (B). Figure adapted from Ref. [25]. The nomenclature, VO_x, is used such that *x* is the number of oxygens from the gas phase that are not part of the CeO_2 (1 1 1) surface.

The band at 850 cm^{-1} may be attributable to V=O vibrations for a vanadate group in which V is connected to the ceria domain through three bridging oxygen atoms, as illustrated for Structure B in Fig. 2. DFT calculations of the spectrum for this structure formed on the (1 1 1) surface of CeO_2 exhibit a band at 876 cm^{-1} [25]. The proposed assignment of the band at 850 cm^{-1} is further supported by work on bilayered $VO_x/CeO_2/SiO_2$ catalysts, in which a broad peak at 850 cm^{-1} was observed upon heating the sample to 773 K. Raising the temperature to 1073 K caused this feature to

Table 1
Surface areas of CeO_x/SBA-15 with V and Ce weight percentages and surface coverages.

Sample name	V, wt.%	Ce, wt.%	CeO_x/SBA-15 surface areas (Ce-free), m^2 g^{-1}	V coverage, V nm^{-2}	Ce coverage, Ce nm^{-2}
V19CetBS	2.9	2.6	589 (687)	0.6	0.2
V51CetBS	2.6	6.1	516 (817)	0.6	0.5
V85CetBS	2.7	8.7	436 (735)	0.7	0.9

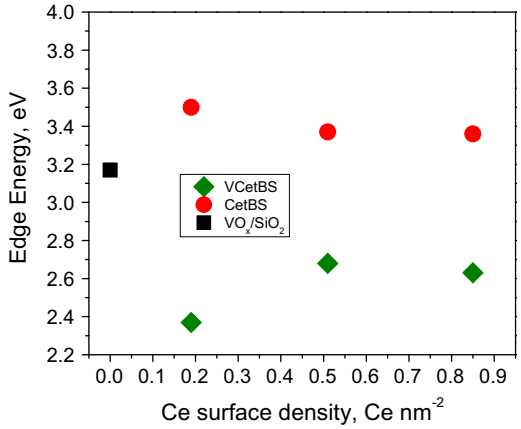

Fig. 3. UV–Visible absorption edge energies for $VO_x/CeO_2/SiO_2$ catalysts. Data were acquired at ambient temperature without exposing samples to moisture.

narrow into an intense peak at 853 cm^{-1} characteristic of $CeVO_4$ formation [16,17]. Thus, the band at 850 cm^{-1} observed in the present study could be a precursor to $CeVO_4$; however, no evidence was observed for $CeVO_4$ in the spectra of VCetBS as indicated by the absence of peaks at 853, 780, and 790 cm^{-1} characteristic of $CeVO_4$. The spectra presented in Fig. 1 also show no evidence for V_2O_5, which has bands at 998, 702, 529, or 287 cm^{-1} [8].

3.1.2. UV–Visible spectroscopy

The UV–Visible edge energies for catalysts with and without V grafted are shown in Fig. 3. The edge energy for the CeO_2/SBA-15 samples is ~3.4 eV, independent of the CeO_x surface density. After V grafting, the edge energy decreased by 0.7–1.0 eV to ~2.6 eV. This edge energy is also lower than that for tetrahedral vanadates on silica, 3.17 eV [5]. The observation of an edge energy for the bilayered catalysts lower than that for either VO_x/SiO_2 or CeO_x/SiO_2 is presumed to be due to the presence of V—O—Ce bonds.

3.1.3. XANES

The V K-edge XANES spectra acquired at ambient temperature are shown in Fig. 4A. The large pre-edge feature for all samples occurs because of hybridization between the O 2p and V 3d orbitals in a non-centrosymmetric environment [39] and indicates predominantly tetrahedral or pseudo-tetrahedral V species on the surface. This conclusion is supported by the examination of the XANES spectra for V^{5+} standards presented in Fig. 4B, which show that as the vanadia environment changes from square pyramidal, V_2O_5, to distorted tetrahedral, NH_4VO_3, to tetrahedral, $CeVO_4$ [40], the pre-edge feature increases as a result of increasing p–d orbital hybridization. Agreement of the edge energy for the VCetBS samples (Fig. 4A) with that for V^{5+} standards (Fig. 4B) further supports the conclusion that all of the V in these samples is in the 5+ oxidation state. Electron paramagnetic resonance (EPR) spectra of VCetBS samples were also acquired, and these showed no evidence for a signal attributable to V^{4+} (data not shown) [41].

3.1.4. MeOH temperature-programmed desorption (TPD)

The catalysts were further characterized by taking TPD spectra of adsorbed MeOH. Fig. 5 illustrates the MeOH, CH_2O, and CH_4 profiles observed for samples of V19CetBS, V51CetBS, V85CetBS, and 85CetBS. In addition to these products, the formation of H_2O, CO, and CO_2 was observed. The spectra for these products are shown in the Supporting Information. Infrared absorption data for these catalysts indicate that methanol initially adsorbs dissociatively producing methoxy and hydroxyl groups bound to Si, Ce, and V

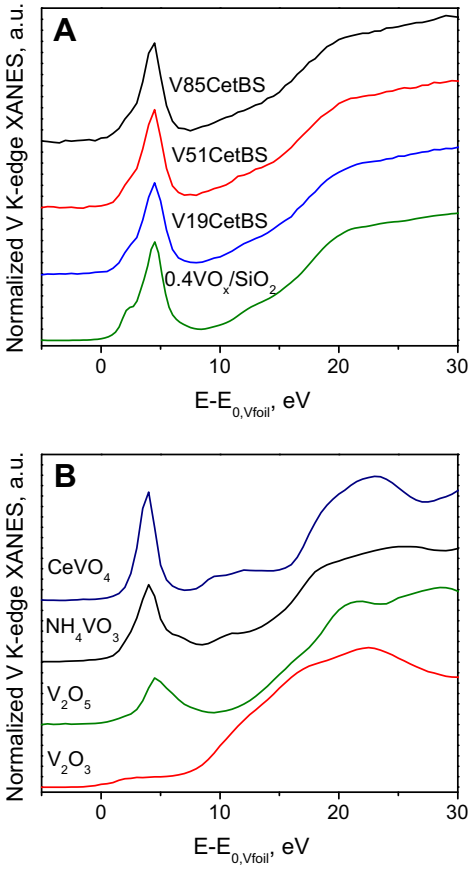

Fig. 4. V K-edge XANES acquired at ambient temperature under He for VCetBS catalysts (A) and V standards (B). The energy is referenced to the initial peak of the V foil derivative spectrum (0 eV).

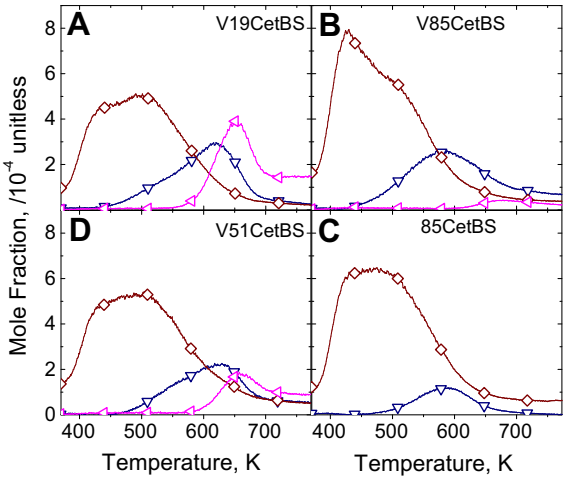

Fig. 5. Temperature-programmed desorption (TPD) profiles for selected catalysts for the following species: MeOH (burgundy diamonds), formaldehyde (blue down triangles), and CH_4 (pink left triangles). Data are normalized to sample mass. (For interpretation of the references to color in this figure legend, the reader is referred to the web version of this article.)

(data not shown), as observed previously for silica- and ceria-supported vanadia [42,3,19].

For all catalysts, MeOH desorbs at 363 K, a temperature well below that for the appearance of any other products. A broad desorption peak for CH_2O begins around 415 K for catalysts

containing V. It is noted that in the absence of V, the appearance of formaldehyde occurs at a temperature of ~50 K higher than for the corresponding VCetBS samples (compare spectra for 85CetBS and V85CetBS). As the Ce surface density increases, the intensity of the formaldehyde profile at 625 K decreases with a concomitant decrease in the production of methane. No methane is observed for CetBS samples. The formation of methane can be attributed to the decomposition of silica-bonded methoxy species that are adjacent to silica-supported mono-vanadate species [3]. While the methane peak temperature for VCetBS catalysts occurs at a slightly higher temperature, ~650 K, than that for VO_x/SiO_2, 625 K [3], the decrease in the quantity of methane formed with increasing ceria surface density and its absence in 85CetBS suggest that methane is produced as a result of isolated VO_x/SiO_2 structures not bound to ceria.

The formaldehyde profiles for VCetBS catalysts are broad, but in every case, the onset of formaldehyde production begins at significantly lower temperatures (~415 K) than that for isolated vanadate species supported on silica (~500 K) [3,43]. A lower formaldehyde production temperature for VO_x/CeO_2 than VO_x/SiO_2 has previously been observed by the group of Vohs and coworkers [20,43]. In these studies, surface coverages of 0.3 and 3.5 V nm^{-2} for VO_x/SiO_2 and 3.4 V nm^{-2} for VO_x/CeO_2 were used, and the peak temperature of formaldehyde desorption decreased from ~675 K for VO_x/SiO_2 [43] to ~600 K or lower for VO_x/CeO_2 [20] (for TPD profiles acquired with a heating rate of 15 K min^{-1}).

3.2. Studies of methanol oxidation

The rates of methanol oxidation on CetBS and VCetBS are shown in Fig. 6 as a function of the ceria surface density. For both sets of samples, the rates are expressed per unit surface area. At 543 K, the ceria layer is active for methanol oxidation, and the rate of formaldehyde production increases linearly with increasing Ce surface density. Under the reaction conditions used, silica shows no activity for methanol oxidation.

After grafting V, the rate of CH_2O formation per unit surface area increases relative to that for CetBS, by about a factor of two. For reference, the rate of formaldehyde formation on VO_x/SiO_2 under equivalent reaction conditions and vanadium loadings is 3.5×10^{-10} mol CH_2O (s m^2)$^{-1}$. Therefore, the high activity of VCetBS is due to the portion of the vanadium interacting with the ceria layer deposited on the SBA-15.

The apparent rate constant for formaldehyde production attributable to vanadia was determined by subtracting the contribution to the CH_2O formation rate due to the ceria layer and dividing the resulting rate per surface area by the methanol vapor pressure and the surface density of vanadia as determined by ICP. As shown in Fig. 7, the VCetBS samples show a constant rate with increasing Ce surface density that is an order of magnitude larger than for $0.3VO_x/SiO_2$ [3]. This increase with Ce surface density is similar in magnitude to that observed in our previous work for $VO_x/TiO_2/SiO_2$ and $VO_x/ZrO_2/SiO_2$ catalysts (~0.6 V nm^{-2}) [4,5], which are also shown in Fig. 7. Taking into account the uncertainty in the data, it can be concluded that the values of k_{app} are very similar to those for $VO_x/TiO_2/SiO_2$, $VO_x/ZrO_2/SiO_2$, and for $VO_x/CeO_2/SiO_2$ once the data are corrected for the activity of the ceria deposit.

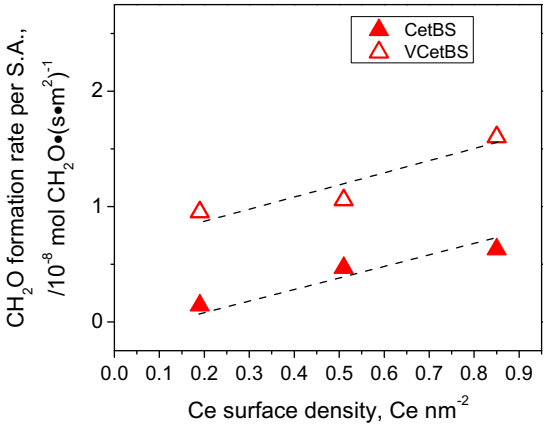

Fig. 6. CH_2O formation rates per surface area of catalyst at 543 K for samples with V (open symbols) and without V (closed symbols). Dashed lines are to guide the eye.

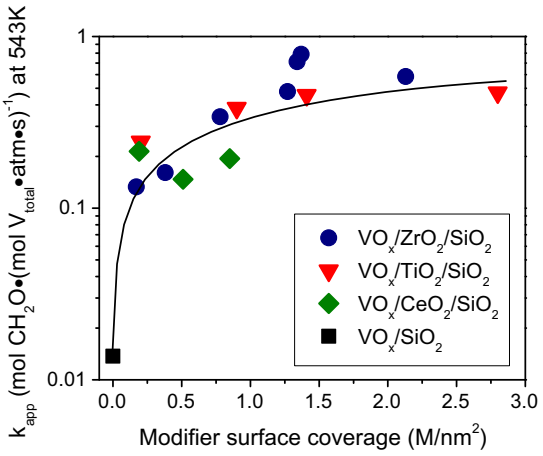

Fig. 7. Apparent rate constants for VCetBS, $VO_x/TiO_2/SiO_2$, and $VO_x/ZrO_2/SiO_2$ catalysts as a function of M surface density (M = Ce, Ti, Zr) at 543 K. Apparent rate constants for $VO_x/TiO_2/SiO_2$ and $VO_x/ZrO_2/SiO_2$ catalysts are from Refs. [4] and [5], respectively. Curve is to guide the eye. $k_{app} = k_2K_1$, where K_1 is the equilibrium constant for Reaction 1 and k_2 is the rate constant for Reaction 2 in Fig. 8.

The apparent activation energy and pre-exponential factor for methanol oxidation on VCetBS catalysts are presented in Table 2. The apparent activation energy is approximately 17 kcal mol^{-1} for all samples. This value is comparable to the activation energy of 18 kcal mol^{-1} for our bulk $CeVO_4$ sample and similar to that reported by Feng et al. for vanadia supported on bulk CeO_2, 16 kcal mol^{-1} [20]. Table 2 also shows that the apparent pre-exponential factor is essentially the same for all samples (~1×10^6 mol CH_2O (mol V atm s)$^{-1}$).

The apparent pre-exponential factors and activation energies obtained in this study are compared with those reported in our work with isolated vanadate species supported on two-dimensional layers of titania and zirconia deposited on silica and with isolated vanadate species supported on silica. As seen in Table 3, activation energies and pre-exponential factors for $VO_x/TiO_2/SiO_2$, $VO_x/ZrO_2/SiO_2$, and $VO_x/CeO_2/SiO_2$ are all very similar and significantly smaller than those for VO_x/SiO_2. A further observation is that both the pre-exponential factor and the activation energy for methanol oxidation occurring on VO_x/SiO_2 are larger than those for the other three catalysts, even though the active form of

Table 2
Apparent pre-exponential factors and activation energies for catalyst samples.

Sample Name	Apparent pre-exponential factor, k^0 (mol CH_2O (mol V atm s)$^{-1}$	Apparent activation energy, E_{app} (kcal mol^{-1})
$0.3VO_x/SiO_2$[a]	2.3×10^7	23
V19CetBS	1.0×10^6	17
V51CetBS	1.0×10^6	17
V85CetBS	2.2×10^6	18

[a] Data from Ref. [3].

Table 3
Apparent pre-exponential factors and activation energies for catalyst samples. In the case of $VO_x/MO_2/SiO_2$ (M = Ti, Zr, Ce), the pre-exponential factor is based on V atoms fully associated with MO_2.

Sample Name	Apparent pre-exponential factor, k^0 (mol CH_2O (mol V atm s)$^{-1}$)	Apparent activation energy, E_{app} (kcal mol^{-1})
VO_x/SiO_2[a]	2.3×10^7	23
$VO_x/TiO_2/SiO_2$[b]	1.8×10^6	18
$VO_x/ZrO_2/SiO_2$[c]	4.0×10^6	16
$VO_x/CeO_2/SiO_2$[d]	2.2×10^6	18

[a] Data from Ref. [3].
[b] Data from Ref. [4].
[c] Data from Ref. [5].
[d] Data for V85CetBS.

vanadia is the same. This suggests that the there may be significant differences in the mechanism by which formaldehyde is formed on $VO_x/TiO_2/SiO_2$, $VO_x/ZrO_2/SiO_2$, and $VO_x/CeO_2/SiO_2$ versus VO_x/SiO_2. This point is discussed in more detail below.

To understand the reason for the increased rate of methanol oxidation on $VO_x/CeO_2/SiO_2$ relative to VO_x/SiO_2, it is useful to first review the mechanism of methanol oxidation proposed for the latter catalyst. Both experimental and theoretical studies suggest that CH_2O is formed via the following sequence of steps [1,3,12,44]. Reaction is initiated by the dissociative adsorption of methanol across a V—O—Si bond to produce V—OCH_3 and Si—OH species. Next, a hydrogen atom from V—OCH_3 is abstracted by the V=O bond of the vanadate species, resulting in the release of CH_2O and the formation of a V—OH species. This step is taken to be rate-determining. Water is then formed by condensation of the V—OH and SiOH groups. Finally, the active site is reoxidized with gas-phase oxygen to return to the fully oxidized initial state [12,3]. Calculations of the enthalpy of methanol adsorption, the apparent activation energy, and the apparent first-order rate coefficient for methanol oxidation were all found to be in close agreement with experiment based on this mechanism [12].

When ceria is present on the surface, the Raman spectra presented here and theoretical studies of the interactions of isolated vanadate species bonded to bulk ceria [25] indicate that the vanadate species are present in the form of VO_3 species (see Fig. 2 and Structure A in Fig. 8). Methanol can then adsorb dissociatively by cleavage of a V—O—Ce bond (Reaction 1 Fig. 8). It is not possible to determine whether the methoxy group is bound to V or Ce because of a single peak in the IR for adsorbed methoxy species and the broad silica absorption band, which obscures the observation of C—O stretches [42]. However, in a previous work by Jehng, a Raman peak was observed at ~1068 cm^{-1} upon methanol adsorption on $VO_x/CeO_2/SiO_2$ catalysts. This feature was attributed to vibrations of V=O bonds in Structure B in Fig. 8 [19,45,46]. Therefore, we assume that methanol adsorption results in the formation of V—OCH_3 and Ce—OH species and that Reaction 1 is quasi-equilibrated. This second assumption is supported by the observation that desorption of methanol via the reverse of Reaction 1, seen in the TPD spectra presented in Fig. 5, occurs at a significantly lower temperature than the conversion of methoxy groups to formaldehyde.

The elementary processes by which V—OCH_3 species react to form CH_2O and H_2O on $VO_x/CeO_2/SiO_2$ cannot be determined directly from the available data. If they were identical to those occurring on VO_x/SiO_2, then one would expect that the oxidation state for V to decrease from 5+ to 3+ and the oxidation state of Ce to remain constant at 4+. If, on the other hand, the transfer of the H atom from V—OCH_3 was to occur via reaction with a Ce—OH group to form CH_2O and H_2O concurrently, then one would expect the oxidation state of V to decrease from 5+ to 4+ and the oxidation state of Ce to decrease from 4+ to 3+.

To gain insight into what species are reduced at temperatures where methanol oxidation occurs, an *in situ* XANES experiment was conducted with V85CetBS. As shown in Fig. 9, the sample was first characterized in He at 300 K. Under this condition, both V and Ce were found to be in their fully oxidized states: V^{5+} and Ce^{4+} [47]. Next, the sample was heated to 600 K in He. Raising the temperature to this level had no effect on the oxidation state of V but resulted in a small amount of Ce undergoing reduction from Ce^{4+} to Ce^{3+} due presumably to the loss of O_2. Exposure of the sample at 600 K to 0.5% methanol in He resulted in a progressive reduction of V^{5+} and Ce^{4+}, with the reduction of ceria occurring more rapidly than the reduction of vanadia. Since CH_2O and H_2O are the only products formed at 600 K, the results of this experiment suggest that the ceria layer to which the vanadate species are bound participates in the formation of the products. We propose that this process may occur via Reaction 2 in Fig. 8. H-abstraction to the ceria domain would initially result in the

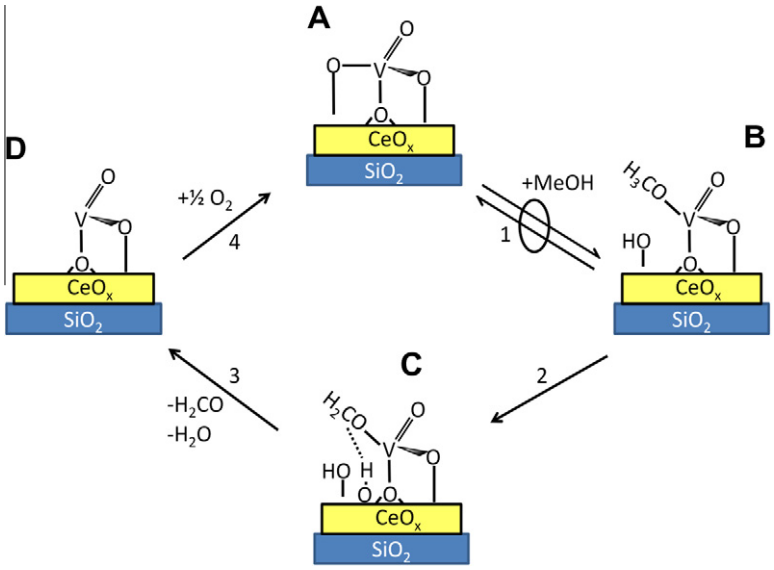

Fig. 8. Proposed mechanism for methanol oxidation on $VO_x/CeO_2/SiO_2$ catalysts derived from the $Ce(O^tBu)_4$ precursor.

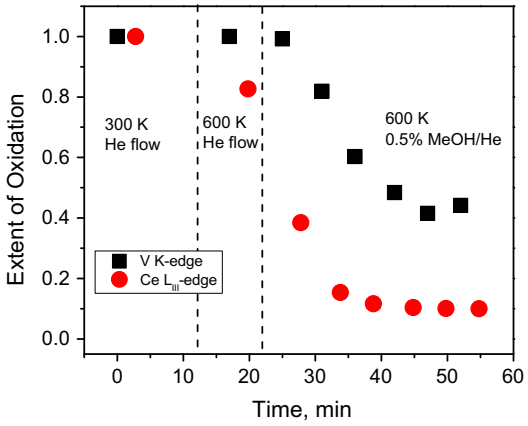

Fig. 9. Extent of oxidation for V K-edge and Ce L_{III}-edge on V85CetBS in He and 0.5%MeOH/He flow. The V K-edge was analyzed by a linear combination fit of the V K-edge under He at 300 K (value of 1.0) and under 5000 ppm methanol flow at 773 K (value of 0.0). The Ce L_{III}-edge was analyzed by the height of the feature at 261.5 eV normalized between the height at 300 K in He (1.0) and the height under methanol flow at 773 K (0.0).

formation of Ce^{3+} and V^{4+} species. Transfer of an electron from the V^{4+} to the ceria layer could then result in the formation of two Ce^{3+} centers (structure D in Fig. 8). A similar mechanism for H-abstraction has been proposed based on DFT calculations of the energetics of methanol oxidation occurring on isolated vanadate species supported on TiO_2(1 1 0) [14].

The reaction mechanism presented in Fig. 8 leads to the conclusion that the apparent first-order rate coefficient for methanol oxidation, k_{app}, is given by

$$k_{app} = k_2 K_1, \quad (1)$$

where K_1 is the equilibrium constant for Reaction 1 and k_2 is the rate constant for Reaction 2. Consistent with this definition, the apparent activation energy, E_{app}, and pre-exponential factor, k^0_{app}, are given by

$$E_{app} = E_2 + \Delta H_1 \quad (2)$$

and

$$k^0_{app} = k^0_2 K^0_1, \quad (3)$$

where ΔH_1 and K^0_1 are the enthalpy change and the pre-exponential factor for the equilibrium constant for Reaction 1, respectively, and E_2 and K^0_2 are the activation energy and pre-exponential factor, respectively, for Reaction 2.

The data presented in Table 3 indicate that the values of K^0_{app} and E_{app} are similar for $VO_x/TiO_2/SiO_2$, $VO_x/ZrO_2/SiO_2$, and $VO_x/CeO_2/SiO_2$ and differ significantly from the corresponding values for VO_x/SiO_2. This then raises the question of whether observed differences in the apparent rate parameters are due solely to difference in the rate parameters for the rate-limiting step, Reaction 2 in Fig. 8 for $VO_x/TiO_2/SiO_2$, $VO_x/ZrO_2/SiO_2$, and $VO_x/CeO_2/SiO_2$ or its equivalent for VO_x/SiO_2, or to a mixture of differences in the equilibrium constants for Reaction 1 and the rate constant for Reaction 2. Some insights into this question can be obtained by examining reported values for the heat of methanol adsorption on isolated vanadate species supported on different metal oxide supports. For bare silica, the initial heat of methanol adsorption has been reported to range from −16 to −19 kcal mol^{-1} [48], which is comparable to that measured on ceria-supported vanadate species, −19 kcal mol^{-1} [20]. While experimental values of the heat of adsorption for isolated vanadate species supported on silica, titania, and zirconia have not been reported, theoretical calculations of the energy for the addition of methanol across a V—O—M (M = Si, Ti, Zr) bond are virtually the same, ~21 kcal/mol [49]. We also observe that the equilibrium constant for methanol adsorption on a monolayer of vanadia supported on SiO_2, Al_2O_3, TiO_2, and CeO_2 does not vary significantly [42]. Taken together, these observations suggest that the observed difference in the activity of $VO_x/TiO_2/SiO_2$, $VO_x/ZrO_2/SiO_2$, and $VO_x/CeO_2/SiO_2$ with respect to VO_x/SiO_2 are less likely due to differences in the equilibrium constant for methanol adsorption than to the differences in rate coefficient for the rate-limiting step. We also note that as the apparent activation decreases, so does the magnitude of the pre-exponential factor (see Table 3), suggesting that there is a compensation effect.

4. Conclusions

Bilayered $VO_x/CeO_2/SiO_2$ catalysts were prepared in which well-dispersed vanadate species were grafted on an amorphous, two-dimensional layer of ceria bonded to SBA-15. The vanadia exists as pseudo-tetrahedral vanadate species bonded to either silica or ceria, with the fraction bound to ceria increasing with ceria surface density. The turnover frequency for methanol oxidation to formaldehyde is about 20-fold higher for $VO_x/CeO_2/SiO_2$ catalysts than for VO_x/SiO_2. The increase in activity is due to the lower activation energy for the rate-determining H-abstraction step from a surface methoxy bound to a V—O—Ce site. This lower activation energy is possible because oxygen bound to ceria adjacent to vanadia abstracts the proton instead of the vanadyl oxygen.

Acknowledgments

The authors would like to thank Dr. Edward Lang and Dr. John Katsoudas for their assistance in operating the beamline at the APS. This work was supported by the Director, Office of Energy Research, Office of Basic Energy Sciences, Chemical Science Division, of the US Department of Energy under Contract No. DE-AC02-05CH11231. Use of the Advanced Photon Source, an Office of Science User Facility operated for the US Department of Energy (DOE) Office of Science by Argonne National Laboratory, was supported by the US DOE under Contract No. DE-AC02-06CH11357.

References

[1] L.J. Burcham, E.I. Wachs, Catal. Today 49 (1999) 467–484.
[2] G. Deo, I.E. Wachs, J. Catal. 146 (1994) 323–334.
[3] J.L. Bronkema, A.T. Bell, J. Phys. Chem. C 111 (2007) 420.
[4] W.C. Vining, A. Goodrow, J. Strunk, A.T. Bell, J. Catal. 270 (2010) 163–171.
[5] W.C. Vining, J. Strunk, A.T. Bell, J. Catal. 281 (2011) 222–230.
[6] J.L. Bronkema, D.C. Leo, A.T. Bell, J. Phys. Chem. C 111 (2007) 14530.
[7] J.L. Bronkema, A.T. Bell, J. Phys. Chem. C 112 (2008) 6404.
[8] X.T. Gao, S.R. Bare, B.M. Weckhuysen, I.E. Wachs, J. Phys. Chem. B 102 (1998) 10842.
[9] X.T. Gao, S.R. Bare, J.L.G. Fierro, I.E. Wachs, J. Phys. Chem. B 103 (1999) 618–629.
[10] X.T. Gao, J.L.G. Fierro, I.E. Wachs, Langmuir 15 (1999) 3169–3178.
[11] A. Goodrow, A.T. Bell, J. Phys. Chem. C 112 (2008) 13204.
[12] A. Goodrow, A.T. Bell, J. Phys. Chem. C 111 (2007) 14753.
[13] H.T. Tian, E.I. Ross, I.E. Wachs, J. Phys. Chem. B 110 (2006) 9593.
[14] H.Y. Kim, H.M. Lee, R.G.S. Pala, H. Metiu, J. Phys. Chem. C 113 (2009) 16083.
[15] H.Y. Kim, H.M. Lee, H. Metiu, J. Phys. Chem. C 114 (2010) 13736–13738.
[16] B.M. Reddy, A. Khan, Y. Yamada, T. Kobayashi, S. Loridant, J.C. Volta, J. Phys. Chem. B 106 (2002) 10964–10972.
[17] B.M. Reddy, P. Lakshmanan, A. Khan, J. Phys. Chem. B 108 (2004) 16855–16863.
[18] B.M. Reddy, K.N. Rao, G.K. Reddy, A. Khan, S.E. Park, J. Phys. Chem. C 111 (2007) 18751.
[19] J.M. Jehng, J. Phys. Chem. B 102 (1998) 5816.
[20] T. Feng, J.M. Vohs, J. Catal. 221 (2004) 619.
[21] J.M. Vohs, T. Feng, G.S. Wong, Catal. Today 85 (2003) 303.
[22] G.S. Wong, M.R. Concepcion, J.M. Vohs, J. Phys. Chem. B 106 (2002) 6451.
[23] G.S. Wong, J.M. Vohs, Surf. Sci. 498 (2002) 266–274.

[24] H.L. Abbott, A. Uhl, M. Baron, Y. Lei, R.J. Meyer, D.J. Stacchiola, O. Bondarchuk, S. Shaikhutdinov, H.J. Freund, J. Catal. 272 (2010) 82–91.
[25] V. Shapovalov, H. Metiu, J. Phys. Chem. C 111 (2007) 14179–14188.
[26] M.V. Ganduglia-Pirovano, C. Popa, J. Sauer, H. Abbott, A. Uhl, M. Baron, D. Stacchiola, O. Bondarchuk, S. Shaikhutdinov, H.J. Freund, J. Am. Chem. Soc. 132 (2010) 2345.
[27] J. Strunk, W.C. Vining, A.T. Bell, J. Phys. Chem. C jp1105746.
[28] D. Zhao, Q. Huo, J. Feng, B.F. Chmelka, G.D. Stucky, J. Am. Chem. Soc. 120 (1998) 6024–6036.
[29] M. Newville, J. Synchrotron Radiat. 8 (2001) 96–100.
[30] B. Ravel, M. Newville, J. Synchrotron Radiat. 12 (2005) 537–541.
[31] J. Rauc, in: J. Tauc (Ed.), Amorphous and Liquid Semiconductors, Plenum, London, 1974.
[32] B.A. Morrow, Spectroscopic Characterization of Heterogeneous Catalysts, Elsevier, New York, NY, 1990.
[33] R.H. Stolen, G.E. Walrafen, J. Chem. Phys. 64 (1976) 2623.
[34] A.D. Murkute, J.E. Jackson, D.J. Miller, J. Catal. 278 (2011) 189–199.
[35] N. Magg, B. Immaraporn, J.B. Giorgi, T. Schroeder, M. Bäumer, J. Döbler, Z. Wu, E. Kondratenko, M. Cherian, M. Baerns, P.C. Stair, J. Sauer, H.J. Freund, J. Catal. 226 (2004) 88.
[36] S. Xie, E. Iglesia, A.T. Bell, Langmuir 16 (2000) 7162.
[37] L.J. Burcham, G. Deo, X. Gao, I.E. Wachs, Top. Catal. 11/12 (2000) 85–100.
[38] C. Popa, M.V. Ganduglia-Pirovano, J. Sauer, J. Phys. Chem. C dx.doi.org/10.1021/jp108185y.
[39] J. Wong, F.W. Lytle, R.P. Messmer, D.H. Maylotte, Phys. Rev. B. 30 (1984) 5596–5610.
[40] G. Bergerhoff, I.D. Brown, in: F.H. Allen et al. (Hrsg.), Crystallographic Databases Chester, International Union of Crystallography, 1987.
[41] R. Cousin, S. Capelle, E. Abi-Aad, D. Courcot, A. Aboukais, Chem. Mater. 13 (2001) 3862.
[42] L.J. Burcham, M. Badlani, I.E. Wachs, J. Catal. 203 (2001) 104.
[43] T. Feng, J.M. Vohs, J. Phys. Chem. B 109 (2005) 2120.
[44] J. Döbler, M. Pritzsche, J. Sauer, J. Am. Chem. Soc. 127 (2005) 10861.
[45] J.M. Jehng, H. Hu, X. Gao, I.E. Wachs, Catal. Today 28 (1996) 335–350.
[46] F.D. Hardcastle, I.E. Wachs, J. Phys. Chem. 95 (1991) 5031.
[47] A. Martinez-Arias, M. Fernandez-Garcia, L.N. Salamanca, R.X. Valenzuela, J.C. Conesa, J. Soria, J. Phys. Chem. B 104 (2000) 4038.
[48] F. Bice, V. Bolis, A. Cavenago, E. Garrone, P. Ugliengo, Langmuir 9 (1993) 2712–2720.
[49] R.Z. Khaliullin, A.T. Bell, J. Phys. Chem. B 106 (2002) 7832–7838.